

High-resolution photoelectron–Auger-electron coincidence study for the L_{23} - $M_{23}M_{23}$ transitions of argon

S. Ricz,¹ Á. Kövér,¹ M. Jurvansuu,² D. Varga,¹ J. Molnár,¹ and S. Aksela²

¹*Institute of Nuclear Research of the Hungarian Academy of Sciences (ATOMKI), Debrecen, P.O. Box 51, H-4001, Hungary*

²*Department of Physical Sciences, University of Oulu, FIN-90014 Oulu, Finland*

(Received 10 September 2001; published 21 March 2002)

We report a high-resolution coincident experiment between the Ar $2p_{1/2}$ and $2p_{3/2}$ photoelectrons and subsequently emitted L_{23} - $M_{23}M_{23}$ Auger electrons, where the $2p$ photoelectrons were ionized far above the threshold. We demonstrate the applicability of the coincidence method when separating the different ionization and decay channels even in the case of strongly overlapping peaks. The measurement was carried out with a new high-energy-resolution electrostatic analyzer that is capable of recording the single and coincidence spectra at large range of emission angles simultaneously. An anomalous value was found for the ${}^2P_{3/2}$ -(${}^3P_{012}/{}^1D_2$) intensity ratio in the $2p_{3/2}$ coincidence spectrum, while all the other relative intensities are in good agreement with the previously published data. The possible reasons for the difference are discussed.

DOI: 10.1103/PhysRevA.65.042707

PACS number(s): 32.80.Fb, 32.80.Hd

I. INTRODUCTION

The high-resolution Auger spectroscopy is a very efficient tool for checking the adequacy of theories in the description of the decaying excited states and the electronic structure of atoms, molecules, and solids. This is especially true, when the instrumental energy resolution is the same or smaller than the natural linewidth of the excited states thus revealing much of the fine structure in the spectra. If the final states of the Auger transitions overlap within their natural widths, it is possible that they cannot be separated, not even with the highest experimental resolution. However, by applying the coincidence technique, relatively clean experimental conditions can be provided for separation of the different excitation and rearrangement processes at high-energy photoionization. This method is very useful, especially for studying the decay of the inner-shell hole at photoionization/excitation in synchrotron radiation experiments. This has been shown recently in the case of the Auger-electron–photoelectron [1,2], Auger-electron–Auger-electron [3,4], Auger-electron–photoion [4], and fluorescent-photon–Auger-electron [5] coincidence experiments. It is also possible to perform complete measurements [6–8], where all parameters describing the photoprocess (matrix elements and their phase-shift differences) are determined.

Many experimental and theoretical studies have been published on the L_{23} - MM Auger spectrum of argon (see, e.g., [9,10], and the references therein). Good agreement among the experimental data for different projectile impact (photon, electron, and ion) verifies the prediction of the two-step hypotheses (the separability of the excitation and relaxation processes). The measured intensities and energies are independent from the mass and charge of the projectile. The existing theories, however, overestimate the transition energies. The deviations are much larger than the uncertainty of the published experimental data. The agreement between the experimental and theoretical data is more or less good for the branching ratios. However, noticeable differences were found between the experiment and the theory for the inten-

sity ratios in the energy region of the L_{23} - $M_{23}M_{23}$ transitions of argon. All theoretical values differ from the measured ones for the ${}^3P_{012}/{}^1D_2$ intensity ratios (see, e.g., Tables 4 and 5 in Ref. [10]). The L_{23} - MM Auger spectrum of argon consists of many overlapping lines, originating from different excitation and rearrangement processes. It may be that some shake-up and/or shake-off satellite lines overlap with the diagram transitions. In spite of the excellent energy resolution of the earlier studies [9,10] where the instrumental resolution (~ 60 meV) was smaller than the natural width of the $2p$ shell of argon ($\Gamma_{2p} \approx 120$ meV), the overlap among the Auger peaks still remains.

Because noncoincident measurements cannot apparently solve the possible satellite contribution on the Ar L_{23} - $M_{23}M_{23}$ Auger spectrum, we decided to detect the Auger electrons in coincidence with $2p_{1/2}$ and $2p_{3/2}$ photoelectrons. Such a measurement seems to be rare in the paper; we could not find any that would include high-kinetic-energy resolution, whole kinetic-energy range of Ar L_{23} - $M_{23}M_{23}$ transitions (200–208 eV), and high photon energy (~ 440 eV). Such measurement is extremely useful in this case because the coincidence condition between the photoelectrons and Auger electrons reduces the overlap between the peaks. Furthermore, because of the high kinetic energy of the photoelectron, the postcollision interaction (PCI) distortion to the line shape is small [11,12]. A recently developed angle resolving electron-electron coincidence spectrometer was used to perform the measurements utilizing simultaneous detection of the single and the coincidence spectra.

II. EXPERIMENT

The measurements were carried out at the beamline I411 [13,14] on the third-generation MAX-II storage ring in MAX-Lab, Lund, Sweden. The main components of the beamline are a hybrid undulator, a modified SX-700 monochromator, and different end stations. The differential pumping stage between the monochromator and the experimental stations maintain the beamline at UHV condition during gas-phase measurements. Before the permanent end station, a 1

m section is reserved for different experimental setups. The usable photon-energy range is 50–1500 eV and the flux is 10^{11} – 10^{13} photons/(s \times 100 mA) at 0.1% bandwidth. The degree of the linear polarization of the light is 98% or better. The used electron analyzer (ESA-22) was mounted at the one-meter section where the horizontal and vertical size of the photon beam was 0.5×1 mm in the target region, respectively.

In order to perform electron-electron coincidence measurements, two spectrometers are needed. In Auger-photoelectron-coincidence spectroscopy [15], one spectrometer is kept fixed to photoelectron kinetic energy and the other is used to scan the Auger kinetic-energy range, yielding an Auger coincidence electron spectrum. During the coincidence measurements also the noncoincidence single spectrum is stored. The electron-electron coincidence measurements are very time consuming due to the limited solid angle of the spectrometers. Furthermore, finding the common sensitive volume of the spectrometers requires serious alignment procedures. In order to overcome these experimental difficulties, a new electron-spectrometer (ESA-22) was developed in ATOMKI, Debrecen in cooperation with the University of Oulu, Finland. The schematic cross section of the spectrometer is shown in Fig. 1.

The analyzer consists of a spherical and a cylindrical mirror. It is very similar to our previously built ESA-21 analyzer [16]. The main difference is that the focal ring can be formed at different diameters, thus, either a series of channeltrons (CHS in Fig. 1) or a position sensitive detector (PSD) can be applied for simultaneous angular recording of electrons. Furthermore, the outer sphere and cylinder are cut into two parts, resulting in two spectrometers, named as 1 and 2. In Fig. 1, OS1 and OC1 sign the outer sphere and cylinder of the spectrometer 1, while OS2 and OC2 are the same for the spectrometer 2. This concept enables us to analyze two independent angularly resolved electron spectra in different energy regions, simultaneously.

At the exit of both spectrometers there are ten channeltrons mounted at every 15° from -75° to 75° relative to the electric vector of the light. Each channeltron can detect electrons within the vertical (φ , see Fig. 1) and horizontal (θ) angular windows of $\pm 1.5^\circ$ and $\pm 5^\circ$, respectively. The angular acceptance of the position sensitive detector is $\pm 1.5^\circ$ (φ) in the vertical direction covering angles from -82.5° to 82.5° with respect to electrical vector with high angular resolution of $\pm 1.5^\circ$. Further advantageous property of the PSD is that the spectrometer works as a spectrograph covering $\pm 0.8\%$ energy band around the selected pass energy. We note that we are not restricted to use only PSD with one spectrometer and channeltrons with the other, but we can also focus the electrons with both spectrometers to the PSD or to the channeltrons.

Both spectrometers share the same inner sphere and inner cylinder. The eccentricity ($\Delta x/r_{\text{outer}}$) and precision of the shape ($\Delta r/r$) of the electrodes are better than 10^{-3} . Δx is the radial displacement between the outer and inner electrodes and r is the radius of the electrodes. It means that the sensitive source volume is the same for both spectrometers within this error. In the present experimental geometry the

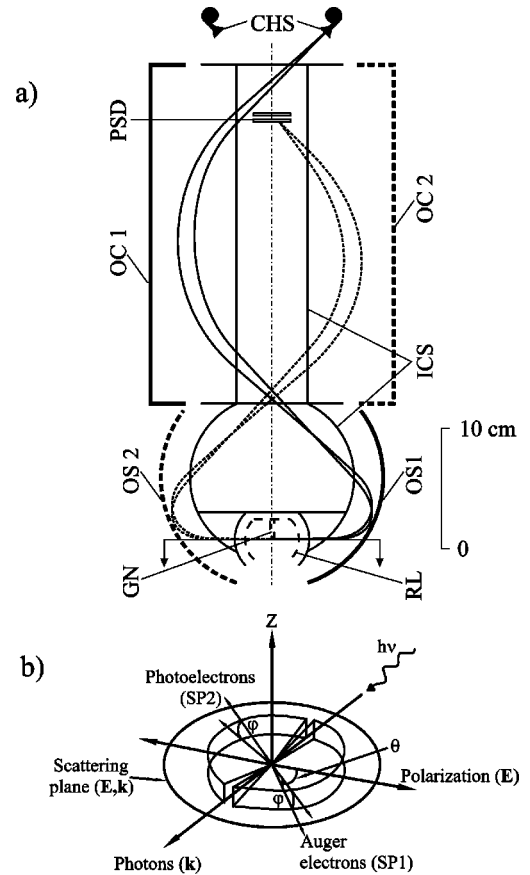


FIG. 1. The schematic cross section of the ESA-22 electron spectrometer (a) and the geometry of the scattering plane (b). The bold dashed and solid lines show the outer electrodes of the spectrometers 1 and 2. The electron trajectories show the two different focusing possibilities. The channeltrons are marked as CHS, position sensitive detector as PSD, outer cylinder and the sphere of the spectrometer 1 as OC1 and OS2, outer cylinder and sphere of the spectrometer 2 as OC2 and OS2, gas nozzle as GN and a spherical retardation lens as RL. θ is the angle between the direction of the electron and the electric vector E of the light, ϕ is the angle between the direction of the electron and the scattering plane (plane of E and k), and k is photon-beam direction.

cylinder axis is parallel to the Z axis as shown in Fig. 1. The analyzer collects the electrons from the *scattering plane*, which is identical with the plane determined by the momentum (\mathbf{k}) and electric (\mathbf{E}) vector of the photon beam. Thus nondipolar effects (see, e.g., Refs. [17,18], and the references therein) to the angular distribution of the electrons can be detected with this setup. Around the target region a spherical retardation lens (RL) was built to increase the energy resolution (RL in Fig. 1). The solid angle of one spectrometer is determined by the slit size of the inner sphere around the scattering plane and it is $\approx 1\%$ relative to 4π in the present setup.

A special gas nozzle was built in the retardation lens to produce beamlike gas target. A piece of a microchannel plate was fixed to the exit of the nozzle with open area diameter of 0.5 mm. The diameter of the target beam is ≈ 3 mm in the scattering plane. It was determined by measuring the size of

the volume of the light emission. The light originated from the outer shells of the target atoms excited by electrons. In the present setup, the sensitive volume of the spectrometer is $\phi 4 \times 1.3$ mm disk and it is higher than the crossed volume of the photon and target beam. It means that the source volume of the spectrometer approximately independent from the angle measured between the direction of the observation and the photon beam.

The above-described advantageous properties of the spectrometer are very useful in electron-electron coincidence studies. The time for the angle-resolved coincidence measurements can be then reduced, which is very important when working at storage ring beamlines where the beam time is limited.

A special measurement control and data-handling system as well as a software was developed for the spectrometer. The high voltages of the spectrometers are controlled by two 18-bit digital-to-analog converter regulated power supplies. The signals from the channeltrons are amplified with two 16-channel voltage-sensitive preamplifiers, and shaped with constant fraction discriminators (3×8 channel) before entering to the so-called single unit. The single unit transforms the fast negative pulse to a positive one and sends them to the 20 *single scalers* and also to the coincidence unit. The coincidence unit forwards the signals to the 20 coincidence scalers if they satisfy the coincidence conditions. The single and coincidence data are stored simultaneously. This solution is very useful in electron-electron coincidence measurement because the single spectrum can be used to correct the raw coincidence data with excellent statistical errors (see details later). The time spectrum originated from the time-to-amplitude converter (TAC) is measured and stored with a multichannel analyzer (MCA). Time spectrum can be used to the estimate of the valid-to-accidental ratio in the coincidence spectrum.

The current coincidence and single measurements were performed at 440 eV photon energy. At this photon energy, the 120 μm monochromator exit slit corresponds to the photon bandwidth of 0.9 eV at beamline I411. The relative energy resolution of the analyzer was set to $\Delta E/E \approx 3 \times 10^{-3}$ and 1.5×10^{-3} for the Auger and photoelectron side, respectively. A constant 100 eV retardation was used to increase the energy resolution. The resulting analyzer energy resolution was 0.3 eV for the Auger electrons and 0.2 eV for the photoelectrons, respectively. The resolution then changes while scanning the Auger spectrum, but only from 0.3 to 0.324 eV in the kinetic-energy range of 199 to 208.5 eV. Such small difference relative to the total resolution is negligible, and do not affect the reliability of the data. Unfortunately we cannot decelerate more, because the time spread caused by different lengths of trajectories of electrons progressively reduce the time resolution at lower kinetic energies.

Photoelectrons were detected with the position-sensitive detector in the -82.5° to $+82.5^\circ$ angular region relative to the polarization vector of the photon beam with the spectrometer 2. The kinetic energy was adjusted so that the whole area of $2p_{1/2}$ or $2p_{3/2}$ photoelectron line illuminated the PSD image. The total experimental resolution (0.92 eV) for the photoelectron lines is clearly better than the difference in

binding energies for the $2p$ spin-split components [$\Delta E_B(2p) = 2.148$ eV [19]], and thus, there was no overlap with the spin-orbit components on the PSD image. The detector efficiency may vary on the detector surface and cause uncertainties to the measurements. This effect was avoided, because the spectrometer 2 voltages were kept constant during the measurements, and so the photoelectron line illuminated the same area on the detector.

In the present experiment, the estimated gas density was a few times 10^{12} atoms/cm³ (it is approximately equivalent with 10^{-3} mbar pressure) in the target beam and the background pressure was 10^{-5} and 5×10^{-6} mbar in the spherical and cylindrical mirror. These conditions are good enough to minimize the multiple scattering of the photons and the ejected electrons in the target and the rest gas region.

The Ar L_{23} - M_{23} M_{23} Auger electrons were detected by channeltrons in the -75° to $+75^\circ$ angular region at every 15° , using the spectrometer 1. The kinetic energy was scanned between 199 and 208.5 eV. The time for one scan with ~ 80 kinetic-energy points was about 30 min and every individual kinetic-energy scan as well as their sum were stored on the computer. The photon flux was measured by a photodiode and its current was transformed to frequency. This signal was led to the counter, and when the selected number of counts was exceeded, the counter was reset and the measurements continued on the next kinetic-energy point. This procedure together with a long lifetime of MAX-II storage ring (flux dropped ≈ 7 mA/h) should ensure that the normalization with the flux was done properly.

The sum signal of the ten channeltrons initiated the TAC and the fast signal taken from the second-channel plate of the PSD was used to stop the TAC. If more than one electron were detected simultaneously by the channeltrons, the sum coincidence unit rejected those pulses and those events were not used to start TAC conversion. The time spectrum of the start-stop pairs was obtained using a multichannel analyzer. The full width at half maximum (FWHM) of the time peak in the spectrum was ~ 12 ns, from which 11 ns originates from the angle-dependent time of flight of the electrons. The ratio of the true and accidental coincidence was 1.8, and the maximum coincidence count rate was 0.13 Hz.

Two separate beam times were used to collect the coincidence data. There was small difference in the analyzer resolution (about 20–40 meV) and in the kinetic-energy step size between the two beam times, but these should have negligible effect to our results considering the branching ratios. Both cases, we could determine the angular distribution of the coincidence Auger spectra because the angle-integrated photoelectron events were used for the coincidence condition.

III. DATA EVALUATION

Due to the finite-time resolution and limited solid angle, the raw coincident data consist of valid and accidental coincidence events. The shape of the random coincidence spectrum should be the same as with the single spectrum. Figure 2 shows the angle-integrated raw coincidence spectra be-

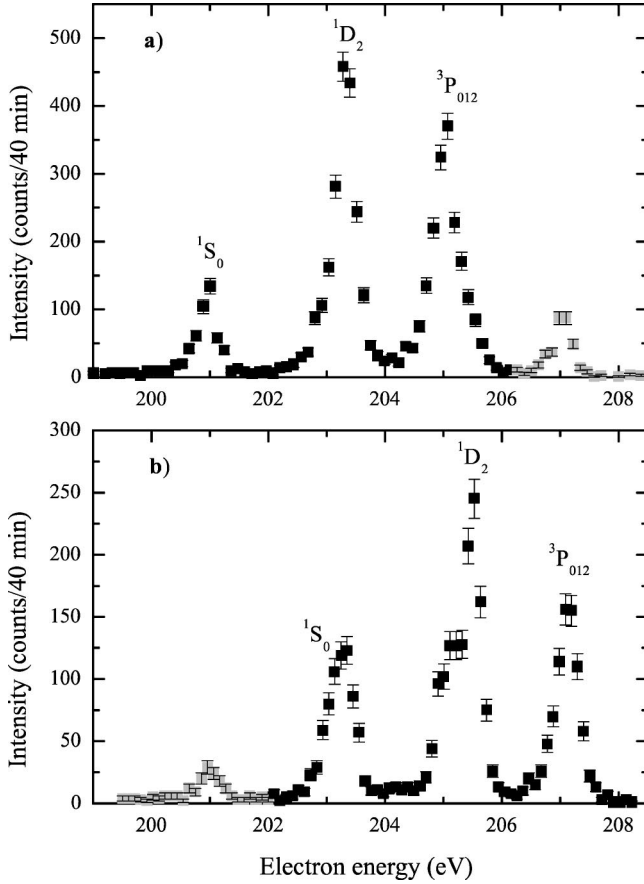


FIG. 2. The figure shows the raw Auger spectra in coincidence with $2p_{3/2}$ (a) and $2p_{1/2}$ (b) photoelectrons. The marked lines belong to the valid coincidence peaks. The light gray part of the spectra was used for the determination of the valid/accidental correction.

tween the $2p_{3/2}$ (a), $2p_{1/2}$ (b), and $L_{23}-M_{23}M_{23}$ Auger electrons.

The accidental coincidence events can be seen clearly in Fig. 2(a), as an appearance of ${}^2P_{1/2}-{}^3P_{012}$ Auger peak at 207 eV. Similarly, the ${}^2P_{3/2}-{}^1S_0$ peak (at 201 eV) is also well visible in Fig. 2(b). For the separation of the valid and accidental coincidence events we determined the ratios of the areas of these peaks from the raw coincidence and single spectra. These values are in good agreement with the valid/accidental ratios obtained from the time spectra. In order to determine the true coincidence spectra, the single spectra were multiplied with these ratios and then subtracted from the raw $2p_{1/2}$, $2p_{3/2}$ coincidence spectra.

For checking the validity of the true coincidence spectra the same procedure was used on the raw coincidence spectra measured at different angles. The angle-dependent accidental correction ratios were determined from the single and coincidence spectra measured at the same angle. The corrected data were integrated for the measured angles. The agreement was excellent between the two spectra obtained with the two methods.

For the determination of the transmission and efficiency of the angular channels (channeltrons) we used the isotropic ${}^2P_{1/2}-{}^3P_{012}$ Auger transition from the single spectra. The A_{20} alignment parameter is zero for the ${}^2P_{1/2}$ intermediate

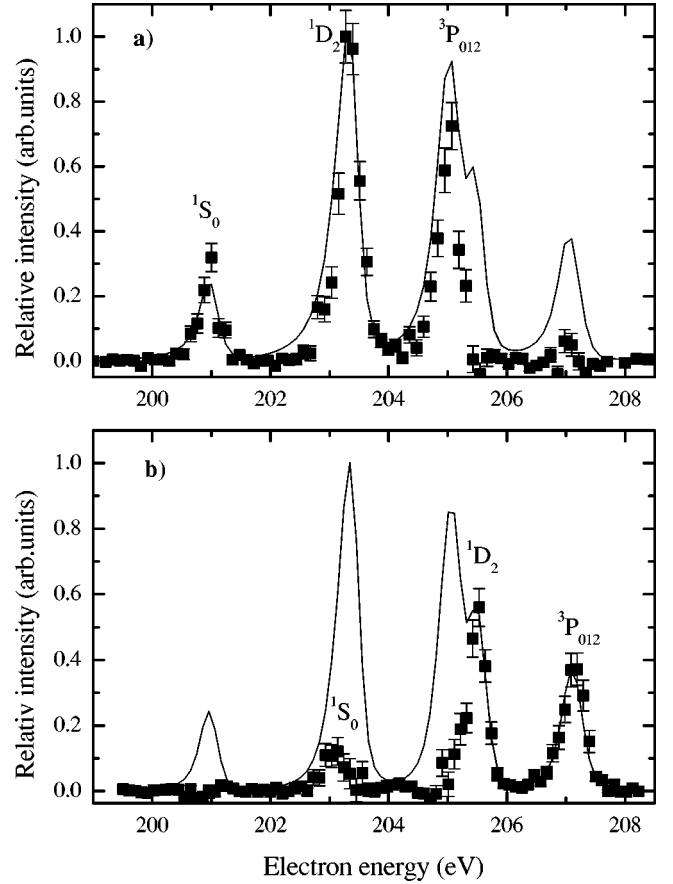


FIG. 3. Comparison between the measured single and true coincidence $L_{23}-M_{23}M_{23}$ Auger spectra of argon. A solid line and full squares with error bars represent the single and the coincidence spectra, respectively. (a) In coincidence with $2p_{3/2}$ photoelectrons, (b) in coincidence with $2p_{1/2}$ photoelectrons. The data were normalized to the ${}^2P_{3/2}-{}^1D_2$, and ${}^2P_{1/2}-{}^3P_{012}$ transitions.

state because the total angular momentum (\mathbf{J}) is less than unity (see, e.g., Refs. [20,21]). Ten noncoincident Auger spectra at different emission angles were fitted with a Voigt function (a convolution of a Lorentzian and a Gaussian function) and using a linear background. The Lorentzian lifetime width was set to 120 meV for all of the peaks, and the FWHM of the Gaussian distribution was linked between the peaks and let to vary freely. From the fit results, the peak areas for the ${}^2P_{1/2}-{}^3P_{012}$ transitions were used to obtain the efficiency factors for each measured angle. These factors were then used to correct the single and coincidence spectra intensities at different angles (different channeltrons). This correction only changes the relative intensities of the spectra at different angles and does not change the branching ratios between the Auger peaks.

IV. RESULTS AND DISCUSSION

Figure 3 shows the measured $L_{23}-M_{23}M_{23}$ single and the random coincidence corrected $2p_{1/2,3/2}$ photoelectron–Auger-electron coincidence spectra of argon at 440 eV photon energy. The Auger data are integrated over the -75° to $+75^\circ$ angular range (sum of ten individual spectra from the

TABLE I. The energies and relative intensities of the $L_{23}\text{-}M_{23}M_{23}$ Auger peaks of argon derived from the coincident (denoted as ‘‘Coinc.’’ in table) and single data.

Final state	Initial state											
	${}^2P_{1/2}$						${}^2P_{3/2}$					
	E^a (eV)	Single ^a	Coinc. ^b	Coinc. ^a	Single ^c	Theory ^c	E^a (eV)	Single ^a	Coinc. ^b	Coinc. ^a	Single ^c	Theory ^c
1S_0	203.10	0.265(7)	0.27(2)	0.26(2)	0.303(7)	0.233	200.97	0.238(2)	0.24(2)	0.27(2)	0.258(8)	0.234
1D_2	205.51	1.0	1.0	1.0	1.0	1.0	203.38	1.0	1.0	1.0	1.0	1.0
${}^3P_{012}$	207.08	0.682(1)	0.82(4)	0.78(4)	0.75(3)	1.07	205.02	0.896(1)	0.66(3)	0.72(3)	0.94(3)	1.26

^aFrom fit.

^bSum.

^cFrom Viktor *et al.* [10].

channeltrons) and photoelectrons were integrated over the -82.5° to $+82.5^\circ$ angle region relative to the electric vector of the light. The solid line is the well-known single Auger spectrum (without coincidence condition), the squares with error bars represent the coincidence data. The single spectra are normalized to the intensity of the ${}^2P_{3/2}\text{-}{}^1D_2$ and ${}^2P_{1/2}\text{-}{}^3P_{012}$ coincidence Auger peaks. Figures 3(a) and 3(b) show clearly that we could eliminate the overlap between the $L_2\text{-}M_{23}M_{23}$ and $L_3\text{-}M_{23}M_{23}$ Auger transitions in the coincident spectrum.

Table I compares relative intensities from our measurements with the earlier single data published by Viktor *et al.* [10]. The coincident ratios were derived by two ways. One of them is the simple sum of the counts of the well-separated Auger peaks and the other one is the results of the fit (see the preceding paragraph). The single and coincidence intensity ratios agree well for all transitions except for the ${}^2P_{3/2}\text{-}({}^3P_{012}/{}^1D_2)$ ratio. This value is 0.92 Ref. [9] and 0.94 Ref. [10] for photon and electron bombardment without coincidence condition, respectively. We obtained ratios 0.896

± 0.001 for the single and 0.66 ± 0.06 for the coincidence spectrum, respectively. Statistical accuracy is very good in our single measurements, since the Auger peak intensity is of order of 10^6 counts. Similar value (0.5 ± 0.1) was also found for the ${}^2P_{3/2}\text{-}({}^3P_{012}/{}^1D_2)$ coincidence intensity ratio in our earlier test measurements with moderate-energy resolution at 350 eV photon energy. The kinetic-energy range was then much narrower and the quality of the data was worse, but this finding is in good agreement with our current result. The coincidence value 0.66 ± 0.06 is about 30% lower than the present and earlier published single experimental ratios. Even larger difference (50%) was found in comparison between the coincidence and theoretical values (see Table I). However, we note that all theoretical calculations published in the paper overestimate these ratios for the ${}^2P_{1/2}$ and ${}^2P_{3/2}$ initial states.

Without coincidence condition, the Auger-electron spectrum is the composition of the following processes (E^k represents the kinetic energy of the photoelectrons, Coster-Kronig transition is signed by CK),

$$h\nu(440 \text{ eV}) + \text{Ar} \rightarrow e_{\text{photo}} \times \left\{ \begin{array}{l} E^k(2p_{1/2}) = 189.4 \text{ eV} \\ E^k(2p_{3/2}) = 191.6 \text{ eV} \end{array} \right\} + \text{Ar}^+ \rightarrow e_{\text{Auger}} + \text{Ar}^{2+}, \quad (1)$$

$$h\nu(440 \text{ eV}) + \text{Ar} \rightarrow e_{\text{photo}} \times \left\{ \begin{array}{l} E^k(2p_{1/2}) = 189.4 \text{ eV} \\ E^k(2p_{3/2}) = 191.6 \text{ eV} - E(3s, 3p \rightarrow nl) \end{array} \right\} + \text{Ar}^{+*} \rightarrow \left\{ \begin{array}{l} e_{\text{Auger}} + \text{Ar}^{2+*} \quad (\text{spectator}) \\ e_{\text{Auger}} + \text{Ar}^{2+} \quad (\text{participator}), \end{array} \right. \quad (2a)$$

$$h\nu(440 \text{ eV}) + \text{Ar} \rightarrow e_{\text{photo}} \times \{E^k(2s_{1/2}) = 113.7 \text{ eV}\} + \text{Ar}^+ \rightarrow e_{\text{CK}} + \text{Ar}^{2+} \rightarrow e_{\text{Auger}} + \text{Ar}^{3+}, \quad (3)$$

$$h\nu(440 \text{ eV}) + \text{Ar} \rightarrow e_{\text{photo}} \times \{E^k(2s_{1/2}) = 113.7 \text{ eV} - E(3s, 3p \rightarrow nl)\} + \text{Ar}^{+*}(nl) \rightarrow \left\{ \begin{array}{l} e_{\text{CK}} + \text{Ar}^{2+*} \rightarrow e_{\text{Auger}} + \text{Ar}^{3+*} \quad (\text{CK spectator, Auger spectator}) \\ e_{\text{CK}} + \text{Ar}^{2+*} \rightarrow e_{\text{Auger}} + \text{Ar}^{3+} \quad (\text{CK spectator, Auger participator}) \\ e_{\text{CK}} + \text{Ar}^{2+} \rightarrow e_{\text{Auger}} + \text{Ar}^{3+} \quad (\text{CK participator}). \end{array} \right. \quad (4a)$$

$$\rightarrow \left\{ \begin{array}{l} e_{\text{CK}} + \text{Ar}^{2+*} \rightarrow e_{\text{Auger}} + \text{Ar}^{3+} \quad (\text{CK spectator, Auger participator}) \\ e_{\text{CK}} + \text{Ar}^{2+} \rightarrow e_{\text{Auger}} + \text{Ar}^{3+} \quad (\text{CK participator}). \end{array} \right. \quad (4b)$$

$$\rightarrow \left\{ \begin{array}{l} e_{\text{CK}} + \text{Ar}^{2+*} \rightarrow e_{\text{Auger}} + \text{Ar}^{3+*} \quad (\text{CK spectator, Auger spectator}) \\ e_{\text{CK}} + \text{Ar}^{2+*} \rightarrow e_{\text{Auger}} + \text{Ar}^{3+} \quad (\text{CK spectator, Auger participator}) \\ e_{\text{CK}} + \text{Ar}^{2+} \rightarrow e_{\text{Auger}} + \text{Ar}^{3+} \quad (\text{CK participator}). \end{array} \right. \quad (4c)$$

In process 1, the Ar atoms are ionized with 440 eV photons, leading to a core hole vacancy in either $2p_{1/2}$ or in the $2p_{3/2}$ subshell. In this scheme, the intermediate-state decays via $L_{23}-M_{23}M_{23}$, $L_{23}-M_1M_{23}$, and $L_{23}-M_1M_1$ Auger transitions. The main interest in this study is the kinetic-energy range of $L_{23}-M_{23}M_{23}$ transitions at 200–208 eV. In our coincidence measurements, we selected photoelectrons that had kinetic energies corresponding to scheme 1. This rules out all other possible initial states as described in processes 2, 3, and 4, because the photoelectron kinetic energy is then different. As a result of this, we can observe only final states that have decayed from $2p$ hole state without initial-state shake processes. However, if the shake up or shake off occurs during the Auger decay, it will be detected because the photoelectron energy is not changed. In noncoincidence measurement of Auger electrons the situation is different. All possible decay channels that produce final states to the kinetic-energy range of $L_{23}-M_{23}M_{23}$ are detected.

Processes 1 and 3 show the $2p$ and $2s$ photoionization with the diagram or cascade Auger transitions, respectively. We note that the $2p$ photoionization with shake off from the M shell produce similar $L_{23}(M)-MM(M)$ Auger spectrum as in process 3 (hole in the subshell is indicated in brackets). Kylli *et al.* [22] studied the argon cascade and shake-off satellite Auger transitions in the $L-MM$ spectra. The measured and calculated energies of the $L_{23}(M_{23})-MM(M_{23})$ transitions are located between 150–201 eV, while the calculated $L_{23}(M_1)-MM(M_1)$ transitions give many weak overlapping lines in the 175–217 eV energy range due to the strong initial and final ionic-state configuration interaction. However, they could not find any peaks corresponding to the calculated $L_{23}(M_1)-MM(M_1)$ Auger transitions in the experimental spectra. Their conclusion was that these transitions produce only a backgroundlike continuous electron spectra. Accepting their results, we believe that the cascade and shake-off processes do not produce any peaks in the energy region of the $L_{23}-M_{23}M_{23}$ transitions. Therefore, these processes are not likely to create any structure of spectra that would explain the difference between the single and coincidence intensity ratios of our measurements.

Processes 2 and 4 describe the $2p$ and $2s$ photoionization with shake up and with the subsequent rearrangement processes, respectively. The energy of the emitted photoelectron is much lower than in the cases of 1 and 3 [the excitation energy $E(3s,3p \rightarrow nl) > 10$ eV]. It means, that the energy of these shake-up peaks are far from the energy of the main photoelectron line so they do not give any contribution to the coincidence spectrum. The decay processes 2(b) and 4(b), 4(c) produce higher- and lower-energy peaks relative to the diagram $L_{23}-M_{23}M_{23}$ transitions, therefore, they do not play any role in the single and coincidence spectra in the measured energy region.

Only the 2(a) and 4(a) decay processes may produce Auger lines in our energy region. However, Pulkkinen *et al.* [9] and Víkor *et al.* [10] investigating the $L-MM$ Auger spectrum of Ar with very high instrumental energy resolution (~ 60 meV), did not observe any extra peaks between energies 200

and 209 eV. Furthermore, the measurement carried out by Pulkkinen *et al.* was at 265 eV photon energy, which is lower than the shake-up and shake-off thresholds [23,24]. Their intensity ratios agree very well with Víkor *et al.* and the present single ratios (see Table I in this paper and Table 3 in the paper by Pulkkinen *et al.*). Therefore the $2p^{-1}3s^{-1}nl$ or $2p^{-1}3p^{-1}nl$ shake-up processes are probably not responsible for the difference between the single and coincidence intensity ratios.

Another possible interpretation of the anomalous coincidence ratio is the difference of the angular distribution between the 1D_2 and $^3P_{012}$ transitions. Arp *et al.* [25] found angular correlation between $K\alpha$ photons and $L_{23}-M_{23}M_{23}$ Auger electrons. In their experiment, x-ray photons were used to create a core hole vacancy in the $1s$ shell. When the $2p$ electron fills the $1s$ hole, a fluorescence photon is emitted. The $2p$ hole is an initial state for the Auger decay and the situation is similar as with the direct photoionization of the $2p$ shell. In their experiment, the $L_{23}-M_{23}M_{23}$ Auger electrons were measured in coincidence with a fluorescence photon. As a result of anisotropical angle distribution in the Auger decay from L_3 initial state, they could observe a difference of order of 5–20% in relative peak intensities when comparing the Auger coincidence spectrum with the isotropic single spectrum. To check similar effect from our data we have determined the angular distribution of the $^2P_{3/2}-(^1D_2, ^3P_{012})$ Auger peaks from the coincidence data. The anisotropy parameters and the intensities were fitted to the experimental data using Eq. (7) in Ref. [26]. The obtained intensity ratio remained 0.64 ± 0.06 from the fit. This value agrees very well with the simple-summed value 0.66 ± 0.03 presented in Table I. Thus the anisotropic angular distribution does not explain the discrepancy between the single and coincidence data in the angular range of our measurements.

Another aspect is that the detection of the photoelectrons and Auger electrons was performed in such angles that the nondipole effects to the angle distribution are possible. However, the magnitude of this effect is likely to be minor compared to the normal dipolelike angle distribution and can be considered negligible [17,27].

In experimental point of view the main difference between the single and coincidence measurement was that in the coincidence case the photoelectrons and Auger electrons were detected in the opposite directions, therefore, the interaction between the photoelectron and Auger electron was strongly reduced [11,12]. This interaction could play an important role in the noncoincidence case.

V. CONCLUSIONS

The high energy-resolution photoelectron–Auger-electron coincidence study of Ar has been reported to demonstrate the applicability of the coincidence method in order to separate the different ionization and decay channels even in the case of strongly overlapping peaks. The $L_{23}-M_{23}M_{23}$ Auger tran-

sitions of argon were measured in coincidence with the $2p_{1/2}$ and $2p_{3/2}$ photoelectrons at 440-eV photon energy. The investigation was carried out with a new high energy-resolution electrostatic analyzer that enabled measurement of the single and coincidence spectra at different angles simultaneously.

Our data were compared with the theoretical and experimental values from the literature. An anomalous intensity ratio for the ${}^2P_{3/2}$ -(${}^3P_{012}$, 1D_2) transitions was found in the coincidence spectrum. The ratio obtained from our single spectrum agrees well with the previous experimental data. We could not interpret the reason for the difference between the single and coincidence intensity ratio with the contribu-

tion of the shake processes to the single spectrum or by the anisotropic angular distribution of the coincidence spectrum.

ACKNOWLEDGMENTS

The authors thank the MAX-Lab staff for providing excellent working conditions. This work was supported by the Synchrotron Committee of the Hungarian National Committee for Technological Development (OMFB), Hungarian Scientific Research Foundation (OTKA No. T025325), the Finnish Academy for the Natural Sciences, Finnish National Graduate School in Materials Physics (NGSMP), and by the European Community-Access to Research Infrastructure action of the Improving Human Potential Program.

-
- [1] P. Lablanquie, F. Penent, R. I. Hall, H. Kjedsen, J. H. D. Eland, A. Muehleisen, P. Pelicon, Ž. Šmit, M. Žitnik, and F. Koike, *Phys. Rev. Lett.* **84**, 47 (2000).
- [2] M. Neeb, J.-E. Rubensson, M. Biermann, and W. Eberhardt, *J. Phys. B* **29**, 4381 (1996).
- [3] R. Wehlitz, L. S. Pibida, J. C. Levin, and I. A. Sellin, *Phys. Rev. A* **59**, 421 (1999).
- [4] U. Alkemper, J. Doppelfeld, F. von Busch, *Phys. Rev. A* **56**, 2741 (1997).
- [5] U. Arp, T. LeBrun, S. H. Southworth, M. A. MacDonald, and M. Jung, *Phys. Rev. A* **55**, 4273 (1997).
- [6] B. Kämmerling and V. Schmidt, *Phys. Rev. Lett.* **67**, 1848 (1991).
- [7] B. Kämmerling and V. Schmidt, *J. Phys. B* **26**, 1141 (1993).
- [8] U. Becker, *J. Electron Spectrosc. Relat. Phenom.* **96**, 105 (1998).
- [9] H. Pulkkinen, S. Aksela, O.-P. Sairanen, A. Hiltunen, and H. Aksela, *J. Phys. B* **29**, 3033 (1996).
- [10] Gy. Viktor, L. Tóth, S. Ricz, Á. Kövér, J. Végh, and B. Sulik, *J. Electron Spectrosc. Relat. Phenom.* **83**, 235 (1997).
- [11] M. Y. Kuchiev and S. A. Sheinermann, *Zh. Eksp. Teor. Fiz.* **90**, 1680 (1986) [*Sov. Phys. JETP* **63**, 986 (1986)].
- [12] P. van der Straten, R. Morgenstern, and A. Niehaus, *Z. Phys. D: At., Mol. Clusters* **8**, 35 (1988).
- [13] M. Bässler, J.-O. Forsell, O. Björneholm, R. Feifel, M. Jurvansuu, S. Aksela, S. Sundin, S. L. Sorensen, R. Nyholm, A. Ausmees, and S. Svensson, *J. Electron Spectrosc. Relat. Phenom.* **101–103**, 953 (1999).
- [14] M. Bässler, A. Ausmees, M. Jurvansuu, R. Feifel, J.-O. Forsell, P. de Tarso Fonseca, A. Kivimäki, S. Sundin, S. L. Sorensen, R. Nyholm, O. Björneholm, S. Aksela, and S. Svensson, *Nucl. Instrum. Methods Phys. Res. A* **469**, 382 (2001).
- [15] H. W. Haak, G. A. Sawatzky, and T. D. Thomas, *Phys. Rev. Lett.* **41**, 1825 (1978).
- [16] D. Varga, I. Kádár, S. Ricz, J. Végh, Á. Kövér, B. Sulik, and D. Berényi, *Nucl. Instrum. Methods Phys. Res. A* **313**, 163 (1992).
- [17] J. W. Cooper, *Phys. Rev. A* **47**, 1841 (1993).
- [18] D. W. Lindle and O. Hemmers, *J. Electron Spectrosc. Relat. Phenom.* **100**, 297 (1999).
- [19] L. Pettersson, J. Nordgren, L. Selander, C. Nordling, K. Siegbahn, and H. Agren, *J. Electron Spectrosc. Relat. Phenom.* **17**, 29 (1982).
- [20] N. M. Kabachnik and I. P. Sazhina, *J. Phys. B* **21**, 267 (1988).
- [21] U. Kleiman, B. Lohmann, and K. Blum, *J. Phys. B* **32**, 309 (1999).
- [22] T. Kylli, H. Aksela, O.-P. Sairanen, A. Hiltunen, and S. Aksela, *J. Phys. B* **30**, 3647 (1997).
- [23] D. J. Bristow, J. S. Tse, and G. M. Bancroft, *Phys. Rev. A* **25**, 1 (1982).
- [24] B. Eriksson, S. Svensson, N. Martensson, and U. Gelius, *J. Phys. B* **21**, 1371 (1988).
- [25] U. Arp, J. W. Cooper, T. LeBrun, S. H. Southworth, M. Jung, and M. A. MacDonald, *J. Phys. B* **29**, L837 (1996).
- [26] N. M. Kabachnik and K. Ueda, *J. Phys. B* **28**, 5013 (1995).
- [27] N. M. Kabachnik and I. P. Sazhina, *J. Phys. B* **29**, L515 (1996).